Received: 27 February 2023 | Accepted: 11 October 2023

DOI: 10.1111/gcb.16994

Global Change Biology WILEY

RESEARCH ARTICLE

Ocean deoxygenation caused non-linear responses in the structure and functioning of benthic ecosystems

Ludovic Pascal[1] | Joannie Cool[1] | Philippe Archambault[2] | Piero Calosi[3] | André L. R. Cuenca[3] | Alfonso O. Mucci[4] | Gwénaëlle Chaillou[1]

[1]Québec Océan, Institut des Sciences de la mer de Rimouski, Université du Québec à Rimouski, Rimouski, Quebec, Canada

[2]Québec Océan, Takuvik, Département de Biologie, Université Laval, Quebec, Quebec, Canada

[3]Québec Océan, Laboratoire de Physiologie Écologique et Évolutive Marine, Département de Biologie, Chimie et Géographie, Université du Québec à Rimouski, Rimouski, Quebec, Canada

[4]GÉOTOP, Department of Earth and Planetary Sciences, McGill University, Montreal, Quebec, Canada

Correspondence
Ludovic Pascal, Québec Océan, Institut des Sciences de la mer de Rimouski, Université du Québec à Rimouski, Rimouski, QC, Canada.
Email: ludovic.pascal@uqar.ca

Funding information
Fonds de recherche du Québec – Nature et technologies, Grant/Award Number: 281864, 285821 and 322485; Marine Environmental Observation Prediction and Response Network, Grant/Award Number: PDF-25-2020; Natural Sciences and Engineering Research Council of Canada, Grant/Award Number: RGPIN-2018-04421, RGPIN-2018-04982, RGPIN-2018-556538 and RGPIN-2020-05627; Réseau Québec Maritime

Abstract

The O_2 content of the global ocean has been declining progressively over the past decades, mainly because of human activities and global warming. Nevertheless, how long-term deoxygenation affects macrobenthic communities, sediment biogeochemistry and their mutual feedback remains poorly understood. Here, we evaluate the response of the benthic assemblages and biogeochemical functioning to decreasing O_2 concentrations along the persistent bottom-water dissolved O_2 gradient of the Estuary and Gulf of St. Lawrence (QC, Canada). We report several of non-linear biodiversity and functional responses to decreasing O_2 concentrations, and identify an O_2 threshold that occurs at approximately at 63 μM. Below this threshold, macrobenthic community assemblages change, and bioturbation rates drastically decrease to near zero. Consequently, the sequence of electron acceptors used to metabolize the sedimentary organic matter is squeezed towards the sediment surface while reduced compounds accumulate closer (as much as 0.5–2.5 cm depending on the compound) to the sediment–water interface. Our results illustrate the capacity of bioturbating species to compensate for the biogeochemical consequences of hypoxia and can help to predict future changes in benthic ecosystems.

KEYWORDS
benthic biodiversity, benthic fluxes, biogeochemistry, bioturbation, hypoxia, nutrients, oxygen, sediment

1 | INTRODUCTION

Oxygen availability is a fundamental environmental factor that influences the physiology, development, behavior, ecology and distribution of living organisms, as well as ecosystem functioning (Diaz & Breitburg, 2009; Levin et al., 2009; Middelburg & Levin, 2009; Spicer, 2016). The O_2 concentration in sea water is determined by a dynamic balance between processes supplying (through photosynthesis, gas exchange across the air-sea interface and advective transport) and depleting O_2 (through biological respiration). When

the rate of O_2 consumption exceeds those supplying it, deoxygenation occurs and can result (at least temporarily) in hypoxia or even anoxia. Hypoxia, a threshold defined here as dissolved O_2 concentrations <62.5 µM (equivalent to 1.42 mL L^{-1} or 2 mg O_2 L^{-1}), naturally occurs in many regions of the world's oceans, typically in coastal areas and semi-enclosed bodies of water with long residence times, high O_2 consumption rates, limited exchanges with O_2-rich waters and strong water column stratification. Over the past five decades, the O_2 content of the ocean has been drastically declining, and the number of documented areas affected by hypoxia has been increasing at an alarming pace (Breitburg et al., 2018; Diaz & Rosenberg, 2008). Water deoxygenation has been aggravated by human activities, mainly through nutrient enrichment and organic matter (OM) discharge leading to an increase in O_2 demand and consumption (Diaz & Rosenberg, 2008; Rabalais et al., 2010) as well as by global warming that reduces O_2 solubility in water and enhances water column stratification thus exacerbating O_2 depletion in bottom waters below a pycnocline (Diaz & Breitburg, 2009; Middelburg & Levin, 2009).

Hypoxia can have far-reaching consequences on sediment biogeochemistry (Middelburg & Levin, 2009). In the sediment, the microbially mediated degradation of OM occurs through the sequential use of electron acceptors according to their energy yields. Following the rapid reduction of O_2 near the sediment–water interface (SWI), nitrate, manganese(IV)- and reactive iron(III)-oxyhydroxides, sulfate and carbon dioxide are sequentially reduced (Froelich et al., 1979; Van Cappellen & Wang, 1996). In coastal sediment, where organic carbon (OC) accumulation rates are high, the vertical sequence is compressed towards the SWI. The decrease of O_2 availability in hypoxic overlying bottom-waters enhances anaerobic pathways and restricts reoxidation processes in the sediment, which leads to the accumulation of reduced compounds near the SWI and their release to the overlying water (Middelburg & Levin, 2009). The first response of benthic organisms to hypoxia is typically behavioral, with mobile species escaping the hypoxic area and less mobile ones adopting specific behaviors, such as emerging to the sediment surface or body elongation (Diaz & Rosenberg, 1995; Riedel et al., 2014, 2016). Depending on the duration and intensity of a deoxygenation event, hypoxia can lead to mortality (Johnson et al., 2021), with hypoxia tolerance being highly species-specific (Diaz & Rosenberg, 1995; Vaquer-Sunyer & Duarte, 2008). The sediments in hypoxic areas are typically characterized by depauperized and functionally poor benthic communities (Levin et al., 2009). Such changes are likely to alter the contribution of the community to the ecosystem functioning (Diaz & Rosenberg, 2008; Snelgrove et al., 2018). An important process in the functioning of benthic ecosystems is bioturbation, defined as animal-driven processes that alter the sediment matrix (Kristensen et al., 2012). By physically mixing the sediment, the fauna influences the distribution of OM and particulate electron acceptors (e.g., iron-oxyhydroxides). Furthermore, by ventilating their burrow, fauna promotes the transport of O_2-rich water into otherwise O_2-poor sediment (i.e., bioirrigation) but also enhances the upward transport of reduced compounds (Volkenborn et al., 2019). Consequently, bioturbation largely influences the whole functioning of ecosystems (Lohrer et al., 2004; Meysman et al., 2006). Under low O_2 conditions, bioturbation activity can be reduced through changes in behavior (i.e., traits-mediated indirect effect) and/or changes in species density and diversity (i.e., density-mediated effect), reducing the transport of oxidized phases that act as an oxidizing barrier that limits the effluxes of toxic reduced compounds to the overlying water (Middelburg & Levin, 2009). In situ studies characterizing the alteration of bioturbation processes in response to (evolutionarily speaking) slow and persistent decreasing O_2 concentrations are, however, very rare (Friedrich et al., 2014; Gammal et al., 2016; Norkko et al., 2019). Yet, the paucity of knowledge about bioturbation coefficients under low O_2 levels represents a major impediment to reliably predicting the sediment response to future decreases in bottom-water O_2 levels (Katsev et al., 2007).

The aim of the present study was to elucidate how macrobenthic community assemblages and sediment biogeochemistry evolve in situ in relation to decreasing bottom-water O_2 concentrations ($[O_2]_{bot}$) with a special focus on bioturbation. In order to achieve our aim, we carried out a biodiversity survey in combination with bioturbation and sediment biogeochemistry assessments in the Estuary and Gulf of St. Lawrence (EGSL). Over the past century, the EGSL has seen its deep-water (>200/250 m) O_2 concentrations decrease from approximately 125 µM in the 1930s to an average of 65 µM for the 1984–2003 period (Gilbert et al., 2005) and down to 35 µM in 2021 (Jutras et al., 2023). In the first decade of this century, persistent hypoxic bottom-waters covered about 1300 km^2 of the EGSL, while this area was estimated to reach 9700 km^2 in 2021 (Gilbert et al., 2005; Jutras et al., 2023). Although eutrophication played a significant role in O_2 depletion between the 1970s and late 1990s, the dominant cause of the bottom-water O_2 depletion since 2008, including the sudden decrease in minimum O_2 levels since 2018, is a change in the circulation in the western North Atlantic, more specifically a change in the relative proportion of the two parental water masses that make up the EGSL bottom-water (Jutras et al., 2020, 2023). The severity of hypoxia is, however, not homogeneous in space, and a landward O_2 concentration gradient exists from relatively normoxic waters in the Gulf to severely hypoxic waters at the head of the Lower St. Lawrence Estuary (Figure 1a). On the other hand, because of the permanent stratification of this deep coastal system, the intensity of hypoxia does not show any detectable seasonal pattern (Jutras et al., 2023). Thus, the EGSL is a unique natural laboratory to study the effect of in situ chronic exposure to different O_2 levels on macrobenthic communities, their bioturbation levels, and sediment biogeochemistry. In addition, using the space-for-time paradigm (Bozinovic et al., 2011; Gaston et al., 2009), this spatial O_2 concentration gradient can be used to further predict the consequences of deoxygenation on the biodiversity and functioning of marine benthic ecosystems. Here, we hypothesize that bottom-water deoxygenation restricts the availability of O_2 at the SWI, resulting in a gradual (1) depletion of most of the thermodynamically favourable electron acceptors and accumulation of reduced compounds within the sediment, and (2) reduction of total density, taxa,

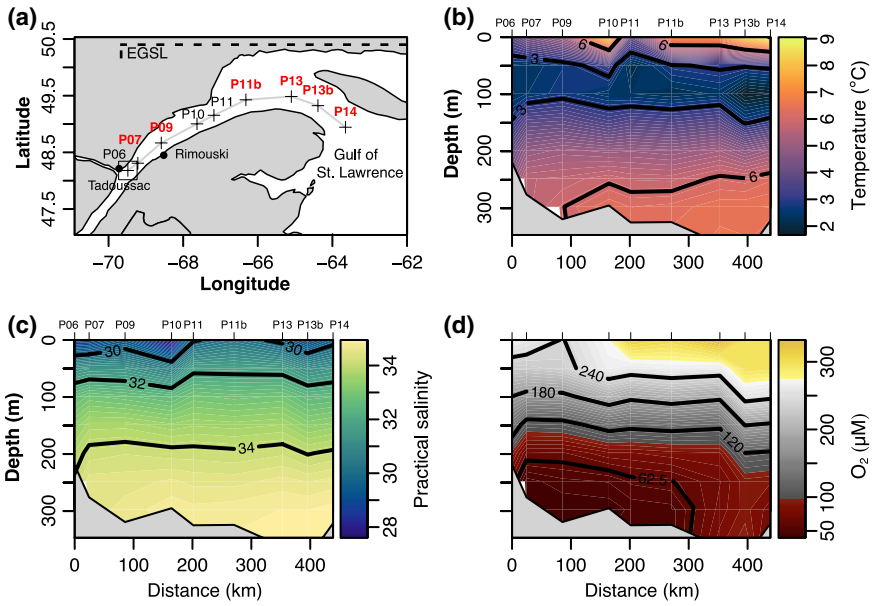

FIGURE 1 Section plots. (a) Location of sampling stations (in red, stations where sediment samples were collected). The dashed line depicts the geographical limits of the Estuary and Gulf of St. Lawrence (EGSL) used in this study, (b) temperature, (c) practical salinity and (d) O_2 concentrations in the water column along the Laurentian Channel (distance is computed from station P06 at the head of the Laurentian Channel). Map lines delineate study areas and do not necessarily depict accepted national boundaries.

and functional richness (FRic) of the macrofauna, and bioturbation rates. Finally, we hypothesize that (3) modifications of sediment biogeochemical dynamics (i.e., vertical distribution of diagenetic compounds and benthic fluxes), as well as of macrobenthic community assemblages and activity, will result in lower total O_2 uptake (TOU) by the sediment.

2 | MATERIALS AND METHODS

2.1 | Study area

The overall water circulation pattern of the EGSL (Figure 1) during the ice-free season is estuarine and described as a three-layer system with warm and brackish surface waters (0–30 m) flowing seaward, these overly a cold intermediate layer (30–150 m deep, formed during winter) that flows landward and sits above warmer and more saline bottom waters that also flow landward (Figure 1). Deep waters are mainly a mixture of cold and O_2-rich Labrador Current Water and warm and O_2-poor North Atlantic Central Waters (NACW). These mix at the edge or on the slope of the continental shelf in the Northwest Atlantic Ocean. The mixing ratio of these water masses has varied over time (Thibodeau et al., 2018) and are currently dominated by NACW (Jutras et al., 2020). The travel time of deep waters from the edge of the continental shelf to the head of the EGSL has been estimated at 3–5 years (Gilbert, 2004). During their journey, the deep waters are isolated from the atmosphere by a permanent pycnocline (Petrie et al., 1996). As a result, O_2 concentrations decrease landward through biological (mostly microbial) respiration and OC remineralization (Gilbert et al., 2005). The OC accumulation rate and the contribution of terrestrial OC to the total sedimentary OC pool, as determined from its stable carbon isotopic composition ($\delta^{13}C$), decrease exponentially seaward (Benoit et al., 2006; Smith & Schafer, 1999).

2.2 | Seawater, sediment, and benthic community sampling design and protocols

Samples were collected from September 14th to 29th, 2020 onboard the R/V *Coriolis II*. A Conductivity-Temperature-Depth sensor (CTD, Seabird SBE 911 plus) and O_2 probe (Seabird SBE-43) mounted on a 12×12 L Niskin-bottle rosette were deployed to record the depth profiles of temperature, practical salinity, pressure, and O_2 concentration throughout the water column at nine stations, from P06 to P14 (Figure 1). Water depths varied between 280 and 390 m (Table 1). Discrete water samples were drawn directly from the Niskin bottles to calibrate the O_2 sensor using Winkler titration, following the procedure described by Grasshoff and Ehrhardt (1999).

Sediment cores were obtained at six stations along the EGSL (Figure 1a). At each station, bottom water (5 m above the sea floor) was collected from the Niskin bottles in airtight plastic bags and stored in the dark at its in situ temperature (ca. 6°C) for later use (Figure 2).

A first set of sediment samples were collected using an Ocean Instrument Mark II box corer (75×75×60 cm). At each station, five large (10 cm inner diam., 40 cm long) and one small (2.5 cm inner diam., 10 cm long) sediment cores were subsampled with transparent acrylic tubing. The level of sediment compression resulting from the tubing insertion was always less than 0.5 cm. The sediment surface within the large sediment cores was immediately capped with Styrofoam, and the tubing was hermetically closed with rubber lids to limit contact with the atmosphere. Within 15 min, sediment cores were transferred to the on-board thermoregulated (6°C) laboratory, gently filled (ca. 1 L *per* core) with the previously retrieved bottom water, connected to an N_2 bubbling system controlled by an O_2 monitoring/regulator device (OXY-REG, Loligo® Systems, Viborg, Denmark), and kept in the dark. Three of the five large sediment cores were kept intact to assess the TOU at the SWI and particle mixing rates (Figure 2). The remaining two large sediment cores were

TABLE 1 Characteristics of sampled stations.

	Water column characteristics				Sediment characteristics				Macrobenthic communities		
Station	Depth (m)	Temp (°C)	Salinity	O_2 (μM)	Mud (%)	LOI (%)	N (%)	C_{org} (%)	$\delta^{13}C_{org}$ (‰)	Total density (ind. m^{-2})	Taxa richness	FRic
P07	281	5.59	34.40	48.7	46.6	4.1	0.07	0.66	−23.8	864 ± 407	18.7 ± 2.5	19.6 ± 4.1
P09	335	5.97	34.55	44.1	93.4	9.0	0.17	1.73	−24.0	565 ± 73	15.3 ± 2.5	16.0 ± 10.4
P11b	330	6.31	34.73	53.8	97.0	10.5	0.19	1.64	−22.4	397 ± 117	16.0 ± 2.6	20.1 ± 2.9
P13	370	6.57	34.90	90.7	97.6	11.1	0.18	1.59	−22.4	731 ± 171	23.7 ± 5.9	29.2 ± 9.8
P13b	390	6.53	34.94	102.8	98.1	11.5	0.21	1.67	−22.5	1176 ± 73	26.3 ± 2.1	30.6 ± 1.7
P14	327	6.48	34.86	84.43	97.4	11.4	0.23	1.78	−22.7	768 ± 293	21.0 ± 1.0	26.0 ± 1.4

Note: Characteristics of the water column (sampling depth and bottom-water temperature, practical salinity, and O_2 concentration), sampled sediment (mud content, loss on ignition [LOI], particulate nitrogen [N], particulate organic carbon [C_{org}] and $\delta^{13}C_{org}$) and macrobenthic communities (total density, taxa richness and functional richness [FRic] given as mean ± SD).

kept intact for O_2 micro-profiling, nutrient pore-water extraction and bioirrigation measurements. The small sediment core was sliced at 0.5, 1, 1.5, 2, 3, 4, and 5 cm for further sediment physical and chemical characterization (see below). Three Van Veen grab sediment samples (0.125 m^2) were recovered to assess the macrobenthic community assemblage.

2.3 | Characterization of the sediment

The sediment grain size was determined by laser diffraction (Malvern Instruments, 2 μm detection limit). The sediment porosity was computed from the water loss after freeze-drying and corrected for the residual sea salt content, calculated from the bottom-water practical salinity, using a dry sediment density of 2.65 g cm^{-3}. The total OM content of the freeze-dried sediment samples was determined from the weight loss on ignition (LOI) at 550°C for 4 h. The organic carbon (C_{org}) and total nitrogen (N_{tot}) content of the surface sediment (0–0.5 cm depth interval) were determined at the GEOTOP facilities (Light stable isotope geochemistry laboratory, GEOTOP-UQAM, Montréal, QC, Canada) using an elemental analyzer (Carlo Erba NC2500). Prior to the C_{org} analysis, inorganic carbon was removed by fuming of sediments in a closed container in the presence of an open beaker concentrated HCl. The C_{org} isotope composition was determined using a Micromass Isoprime 100 isotope ratio mass spectrometer coupled to an Elementar Vario MicroCube elemental analyzer. Carbon isotope ratios are reported on the delta notation, $\delta^{13}C_{org}$, relative to the Pee Dee Belemnite standard.

2.4 | Determination of seawater and pore-water oxygen, and nutrient concentrations

In this study, the diffusive O_2 uptake (DOU) was used as a proxy for the rate of OC mineralization and the reoxidation of reduced diagenetic compounds. Oxygen concentration within the sediment was measured using Clark type microelectrodes. At least five depth profiles of O_2 concentration were carried out at random locations within one large sediment core *per* station. This sampling design was chosen because it has been shown that biogeochemical heterogeneity of the sediment is often associated with microenvironments (Stockdale et al., 2009). Microelectrodes (OX100, Unisense®, Aarhus, Denmark) were inserted into the sediment in 100 μm steps using a motor-driven micromanipulator (MU1, Pyroscience®, Aachen, Germany). A two-point linear calibration of the electrodes was achieved from measurements of the O_2 concentration of air-bubbled bottom water (100% saturation) and the anoxic zone of the sediment (0%). Throughout micro-profiling, an N_2 bubbling system maintained the in situ bottom-water O_2 saturation. Oxygen micro-profiles were typically completed within 30–60 min of core recovery. Oxygen diffusive fluxes (DOU in mmol $m^{-2}h^{-1}$) were computed on the O_2 gradient between 0 and 500 μm depth below the SWI using Fick's first law of diffusion (Equation 1).

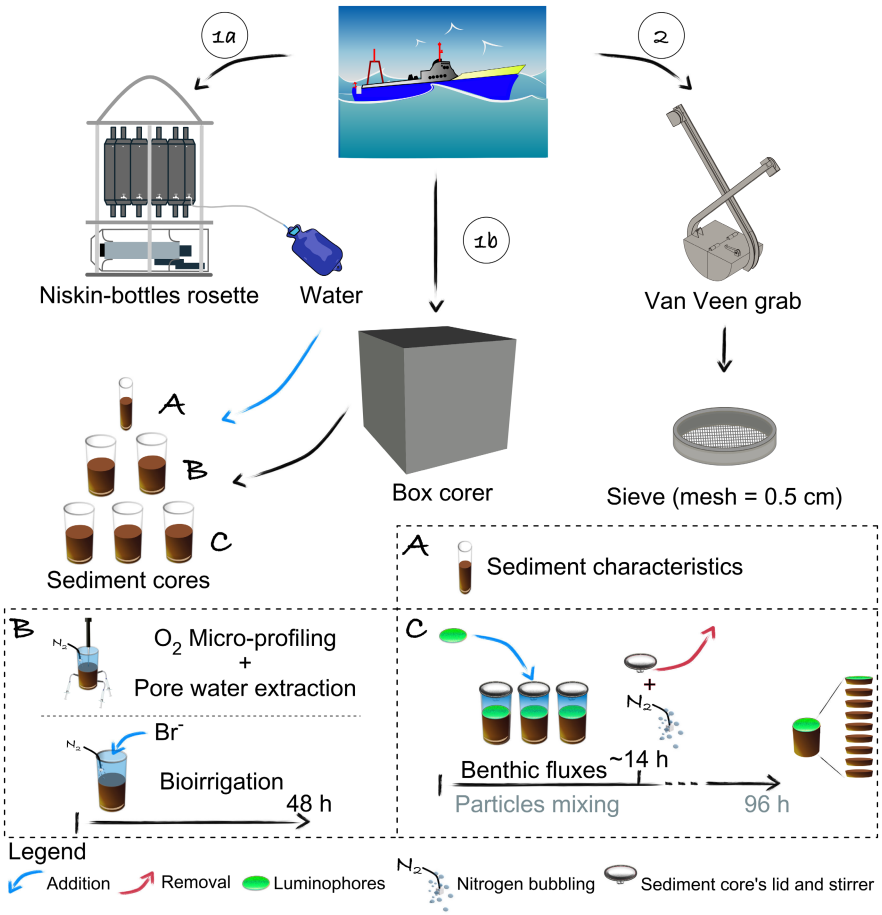

FIGURE 2 Schematic representation of the sampling procedure and experimental design. (1a) First, bottom water was collected and stored in gastight bags. (1b) Six sediment cores were collected with a box corer for (a) sediment characteristics, (b) O_2 micro-profiling, pore-water extraction and bioirrigation assessment and (c) O_2 benthic fluxes and particle mixing measurements. (2) Sediment samples were also collected with a Van Veen grab and sieved through a 1 and a 0.5 mm mesh for macrobenthos identification.

$$\mathrm{DOU} = \phi \times \frac{D_0}{1 - \ln(\phi)^2} \times \frac{\delta C}{\delta z} \quad (1)$$

where ϕ is the sediment porosity, D_0 is the diffusion coefficient ($m^2\,h^{-1}$; computed for each station-specific temperature and salinity according to Boudreau, 1997) of O_2 in water, and $\delta C / \delta z$ is the concentration gradient ($mmol\,m^{-3}\,m^{-1}$). The O_2 penetration depth (OPD), the depth at which O_2 concentration was <1% of the concentration in the overlying water, was estimated from the micro-profiles.

After O_2 micro-profiling, rhizons (Rhizosphere research products) were inserted in the sediment core to extract sediment pore water at 0.5, 1, 1.5, 2, 3, 4, 5, 7 and 10 cm depth. Pore-water samples were stored at −80°C until later nutrient analyses. Pore-water NH_4^+ samples were measured by the colorimetric method described in Grasshoff and Ehrhardt (1999) with a detection limit <1 μM. Nitrite + nitrate (NO_x; detection limit <0.2 μM) and soluble reactive phosphate (SRP; detection limit <0.1 μM) were determined by an AutoAnalyzer 3 HR (Seal-analytical®, Norderstedt, Germany) following the procedures described by Aminot et al. (2009).

2.5 | Determination of bioirrigation levels

Immediately after the addition of previously collected bottom-water, 1 mL of the overlying water was sampled and filtered through a 0.2 μm cellulose membrane to determine the natural dissolved bromide (Br^-) concentration. Thereafter, a known volume of NaBr (1 M) was added to the overlying water of one of the remaining sediment cores to reach an initial concentration of about 10 mM. At the start and at the end of the bioirrigation incubation, 1 mL of the overlying water was similarly sampled. The bioirrigation incubation lasted 48 h, during which the sediment core was connected to the N_2 bubbling system that maintained the $[O_2]_{bot}$ at in situ value and a homogeneous dissolved tracer distribution in the overlying water. At the end of the incubation period, pore-water was sampled with rhizons, as previously described, at 0.5, 1, 1.5, 2, 3, 4, 5, 7 and 10 cm depth below the SWI for bromide analyses. Samples for Br^- were analyzed colorimetrically following the method of Lepore and Barak (2009) with a precision of ±5%. A numerical model was fitted to bromide-depth profiles to estimate the non-local exchange rate, α (min^{-1}), between the overlying water and pore-water (Boudreau, 1984). The Br^- concentration C in the sediment is described by Equation (2), as detailed in Martin and Banta (1992):

$$\phi \times \frac{\delta C}{\delta t} = \frac{\delta}{\delta z}\left(\phi D_s \times \frac{\delta C}{\delta z}\right) - \alpha\phi \times (C - C_{ow}) \quad (2)$$

where ϕ is the porosity, t is time, D_s is the Br^- pore-water diffusion coefficient (computed for each station-specific temperature and salinity according to Boudreau, 1997), z is the sediment depth and C_{ow} is

the bromide concentration in the overlying water. α is assumed to be constant over a fully bioirrigated depth L_b below which the non-local exchange rate decreases exponentially as modulated by the attenuation coefficient $k\alpha$.

$$\alpha(z)=\begin{cases}\alpha, & \text{if } z\le L_b\\ \alpha\times e^{-(z-L_b)/k_\alpha}, & \text{if } z>L_b\end{cases} \quad (3)$$

Modelling was conducted using R software (R Core Team, 2022) and relied on the R package ReacTran (Soetaert & Meysman, 2012) for one dimension transport modelling and the R package deSolve (Soetaert et al., 2010) for solving the Equation (2). α, L_b, and $k\alpha$ were estimated by iteration, minimizing the root mean square error (RMSE) of the predicted tracer profile on observed data. Details of the parameters used for bioirrigation modelling are shown in Table S4.

2.6 | Determination of the total oxygen uptake by the sediment

TOU and particle mixing were assessed on the same set of three sediment cores (Figure 2c). First, 5 g of luminophores (40–60 µm size range, density = 2.5 g cm^{-3}; PARTRAC®, Glasgow, UK) were homogeneously spread at the sediment surface of three sediment cores (*per* station). These sediment cores were then fitted with PVC lids equipped with magnetic stirrers. The dissolved O_2 concentration was measured in real time using an optode (O_2 sensor Spot SP; PreSens®, Regensburg, Germany) connected to a multichannel O_2 meter (OXY-10 SMA; PreSens) through optical fibre cables. A linear calibration of the optode was conducted from the measurements of the O_2 concentration in a bottom-water sample purged with ambient air (100% saturation) and a sodium ascorbate solution (0% saturation). Benthic flux incubations were performed in the dark at the in situ bottom-water temperature. The duration of these incubations was adjusted so that O_2 saturation in the overlying water never fell below 80% of its initial value. The slope (in mmol m^{-3} h^{-1}) from the linear regression of the changes in O_2 concentration over the incubation period was used to compute the TOU, as follows:

$$\text{TOU} = \text{slope}\times\frac{V}{A} \quad (4)$$

where V is the volume of overlying water (m^3), and A is the surface of the SWI (m^2). The TOU by the sediment includes, in addition to DOU, fauna respiration and sediment irrigation (Glud, 2008). In this study, the comparison between TOU and DOU was used to assess the contribution of the macrobenthic community to the TOU.

After the TOU incubations, the sediment cores were opened, and reconnected to the N_2 bubbling system to continue the incubation for the particle mixing assessment.

2.7 | Determination of particle mixing

The particle mixing incubations lasted 4 days (including the duration of benthic flux incubations) before the sediment cores were sliced over the 0.5, 1, 1.5, 2, 3, 4, 5, 6, 8, 10, 12, 15 cm depth interval below the SWI. Sediment slices were freeze-dried and homogenized. From each slice, a 1 g subsample of dry sediment was spread onto a plate and photographed under UV light using a digital camera (α9; SONY®). Luminophores were counted on each image after a binarization step (based on RGB threshold) using Analyze particles function in ImageJ software (ver. 1.53a). The proportions of luminophores in each slice were used to compute depth profiles of luminophores for each sediment core. The maximum penetration depth (MPD) of luminophores (a proxy of mixing depth) was assessed from these profiles. Biodiffusion coefficients (D_b; as a proxy of sediment reworking rates) were estimated using a simple biodiffusive model (Cochran, 1985) to fit the depth profile of luminophore concentration, following Equation (5):

$$\frac{\delta^2 C}{\delta t} = D_b\times\frac{\delta^2 C}{\delta z^2} \quad (5)$$

where C is the luminophore concentration (%), t is the time (year), and z is the vertical depth in the sediment column (cm).

A solution to Equation (6) is:

$$C(z,t)=\frac{M}{\sqrt{\pi D_b t}}e^{\left(\frac{-z^2}{4D_b t}\right)} \quad (6)$$

where M is the amount of available tracers deposited at the sediment surface ($z=0$) at the start of the incubation ($t=0$). D_b was estimated by iteration, minimizing the RMSE of the predicted tracer profile on observed data.

2.8 | Macrofauna identification

Sampled sediment was sieved on-board through 1 and 0.5 mm mesh sieves. The retained material from each fraction was preserved in a 4% buffered formaldehyde-saline solution for later macrofauna identification in the laboratory. Macrobenthic organisms were sorted, counted, and identified to the lowest taxonomic level possible. From this database, total macrofauna density and taxa richness were calculated. In this study, we identified two biological traits (Feeding types and Bioturbation mode) characterized by four categories each to describe the organisms' functional behaviors (Table S1). Taxa were assigned trait modalities using a standard fuzzy coding approach (Chevenet et al., 1994), which allowed each taxon to represent multiple trait modalities and thus account for intraspecific variations. Scoring ranges from 0 to 3 were adopted: with 0 corresponding to no affinity for a given trait modality, 1 and 2 reflecting, respectively, a low and high affinity and 3 an exclusive affinity. Information on trait expression for all taxa were extracted from several sources (Degen

& Faulwetter, 2019; Faulwetter et al., 2014; Queirós et al., 2013). When information was not available for a given taxon, information was obtained from that of closely related species at the nearest taxonomic level. The community trait expression in each sample was computed from the multiplication of the species density matrix by the trait categories matrix. FRic (Villéger et al., 2008) was computed from these two biological traits (i.e., feeding type and bioturbation mode) within a distance-based framework (Laliberté & Legendre, 2010).

2.9 | Data analyses

Data analyses were performed using R software (R Core Team, 2022) (ver. 4.2.0). CTD and dissolved O_2 data from the CTD casts were calibrated, processed and visualized using *oce* package (Kelley & Richards, 2022). Data values are given as means ± SD. First, linear models (lm function from *stats* package) were fitted to test the effects of *Station* (fixed factors; six levels) on the OPD, DOU, total macrofauna density, number of species, FRic, bioturbation metrics (i.e., maximum penetration depth of luminophore, biodiffusion coefficient and nonlocal bioirrigation coefficient), and TOU. The normality and homoscedasticity of the residuals and the presence of outliers were assessed visually for each model. If a significant effect of the *Station* factor was observed ($p < .05$), pairwise tests (Tukey contrast) were performed to characterize their modalities. Second, the nature of the relationship (linear vs. non-linear) between each variable showing significant differences between stations (i.e., all mentioned above except FRic) and $[O_2]_{bot}$ was investigated using generalized additive models (gam function from *mgcv* package; Wood, 2017). The thin plate regression spline smooth class and restricted maximum likelihood were used to fit the model to the data. Station P07, at the head of the EGSL, was removed from the analysis because of its location where distinct environmental conditions (significant mixing with near-surface waters in response to rapid shoaling) are encountered. Tests assumptions were checked as mentioned above.

Macrofauna density data were transformed using Hellinger transformation. Stations were grouped using a hierarchical clustering analysis with a *ward* agglomeration method (hclust function from *stat* package). Patterns of macrobenthic community assemblage were visualized using principal component analysis (PCA, RDA function from *vegan* package; Oksanen et al., 2022). In addition, the difference in macrobenthic community between clusters was tested using a multivariate analysis of variance. The contributions of environmental factors that explain differences in benthic assemblages were investigated using transformed-based redundancy analysis (tb-RDA). Environmental data were standardized and checked for co-correlation using variance inflection factor (VIF) values (environmental factors with VIF greater than 10 were removed from the environmental data matrix). Stepwise selection was used to build models using model R^2 for variable selection. The significance of the tb-RDA overall model, terms, and axes were tested using permutation tests. Patterns of biological trait expressions were visualized using PCA of the Hellinger-transformed data.

3 | RESULTS

3.1 | Water column and sediment characteristics

At the time of sampling, the EGSL hypoxic area was found below 200/250 m depth and extended over ca. 300 km, encompassing station P07, P09 and P11b (Figure 1). The sediment characteristics were relatively similar along the EGSL except at the head (station P07) where sediment was sandier, poorer in OM and had a lower $\delta^{13}C_{org}$ signature (Table 1). Excluding P07, $[O_2]_{bot}$ was the only physico-chemical variable that exhibited significant changes along the EGSL.

3.2 | Oxygen and nutrient pore-water concentrations

Diffusive O_2 fluxes (DOU) were similar at all stations except at P09 where it was about twice as high (Table S2; Figure 3b). DOU was related to $[O_2]_{bot}$ in a significant non-linear fashion (Table S3; Figure 3e) The OPD also significantly differed between stations (Table S2; Figure 3c) and increased (*quasi*) linearly with $[O_2]_{bot}$ (Figure 3f).

Bottom-water and pore-water NO_x, NH_4^+ and SRP concentrations at station P07 were barely detectable except for a relatively small peak in NO_x at the sediment surface (0–0.5 cm depth interval). Along the transect O_2 concentration gradient, NO_x concentrations were always higher in the bottom-waters than in the pore waters. All sediment cores showed a NO_x peak at the sediments surface and decreased sharply to reach below detection limit concentrations around 3 cm deep. The magnitude of the sub-surface pore-water NO_x peak decreased with $[O_2]_{bot}$. At all stations, the bottom-water NH_4^+ concentration was close to the detection limit in the first cm below the SWI. NH_4^+ concentrations increased noticeably with depth in the sediment and the concentration at 10 cm depth decreased with increasing $[O_2]_{bot}$. The bottom-water SRP concentrations were lower than in the pore-water. SRP concentrations increased with depth over the first 10 cm of the sediment column. In the hypoxic area, SRP concentrations were larger and detectable from the sediment surface while SRP concentrations in the non-hypoxic area were smaller, and only detectable below ~3 cm depth beyond which they remained relatively constant until 10 cm depth.

3.3 | Macrobenthic community assemblage

A total of 13,944 individuals from 18 samples (six stations × three replicates) were sorted and 94 taxa were identified. Total density, taxa and FRic of macrobenthic fauna are reported in Table 1. Total density significantly differed between stations (Table S2) and decreased asymptotically with decreasing $[O_2]_{bot}$ (Figure S1) except at

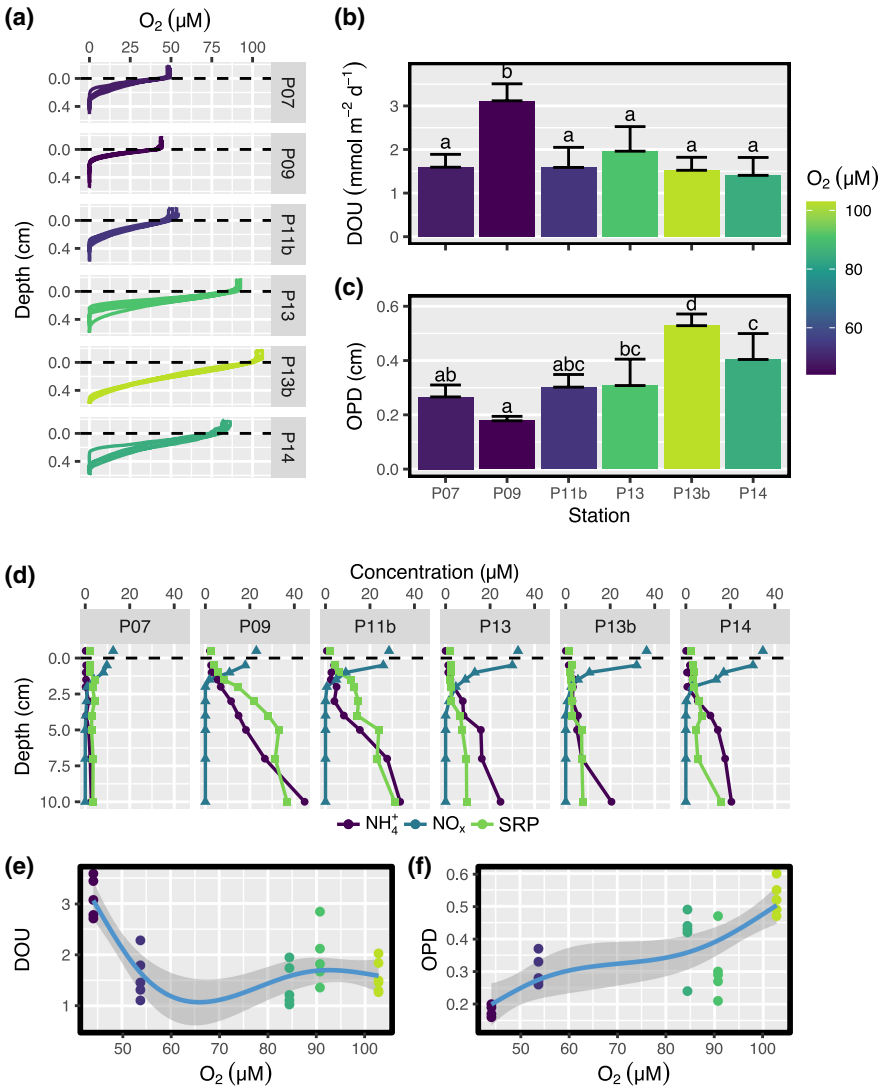

FIGURE 3 Sediment O_2 and nutrient concentrations. (a) Depth profiles of dissolved O_2 concentration in the sediment and associated mean (±SD), (b) diffusive oxygen uptake (DOU; $n = 5$), (c) oxygen penetration depth (OPD; $n = 5$), (d) depth profiles of NO_x, NH_4^+ and soluble reactive phosphate (SRP) and (e, f) generalized additive model plots showing the effect of bottom-water O_2 concentration on both DOU and OPD (station P07 was excluded from this analysis, see text for details). Colour scale defines bottom-water O_2 concentration at the station whilst different letters indicate significant differences between stations.

station P07 where a relatively high total density was recorded. Taxa and FRic decrease linearly with decreasing $[O_2]_{bot}$. When comparing the total density within each size fraction (i.e., >1 mm and 0.5–1 mm), the 0.5–1 mm fraction accounted for 70%–86% of the total density at all stations except at P07 where it only accounted for 27% (Figure S2).

Three groups of stations were discriminated on the basis of hierarchical clustering (Figure 4a). Cluster 1 included the hypoxic stations P09 and P11b, cluster 2 included the non-hypoxic stations P13, P13b and P14 and cluster 3 was comprised of station P07 only. The clustering was statistically justified (df = 1, $F = 5.851$, $p = .001$, $R^2 = 22.2\%$; Figure 4b). The segregation of clusters 1 and 2 from cluster 3 resulted mainly differences in the density of the Polychaeta Spionidae *Ttrochochaeta watsoni* and *Spiophanes kroyeri*, the Polychaeta Sabellidae *Chone* spp., the Sipuncula Golfingiidae *Phascolion* (*Phasocilion*) *strombus strombus* and the Echinodermata Ophiuridae *Ophiura sarsii*, all of which were more abundant in cluster 3, and the density of the Polychaeta Paraonidae *Levinsenia gracilis* which was more abundant in clusters 1 and 2 (Figure 4c). The segregation of cluster 1 from cluster 2 resulted mainly from differences in the density of the Polychaeta Cossuridae *Cossura* spp. and the Polychaeta Nereididae *Ceratocephale loveni* which were more abundant in cluster 1, and the density of the Polychaete Capitellidae *Heteromastus filiformis* which was more abundant in cluster 2. When considering community biological trait expressions, the segregation of clusters 1 and 2 from cluster 3 was confirmed (Figure 4d). This segregation mainly resulted from differences in the density of conveyors, filter feeders and surface deposit feeders which were more abundant in cluster 3. Stations from cluster 2 were overall at the centre of the multivariate space. On the other hand, cluster 1 was divided in two subclusters with samples from station P9 characterized by higher density of surficial modifiers and samples from stations P11b characterized by a higher density of biodiffusers and scavengers.

The variables LOI (df = 1, $F = 20.255$, $p = .001$), $[O_2]_{bot}$ (df = 1, $F = 8.181$, $p = .001$), $\delta^{13}C_{org}$ (df = 1, $F = 4.790$, $p = .004$) and Depth (df = 1, $F = 2.176$, $p = .053$) were used in the model (df = 4, $F = 8.850$, $p = .001$) to construct the tb-RDA based on Hellinger-transformed macrofauna density (Figure 4f). This model explained 64.9% (adjusted R^2) of the total variance. Differences in the macrobenthic community assemblage between clusters 1 and 2 and cluster 3 were mainly related

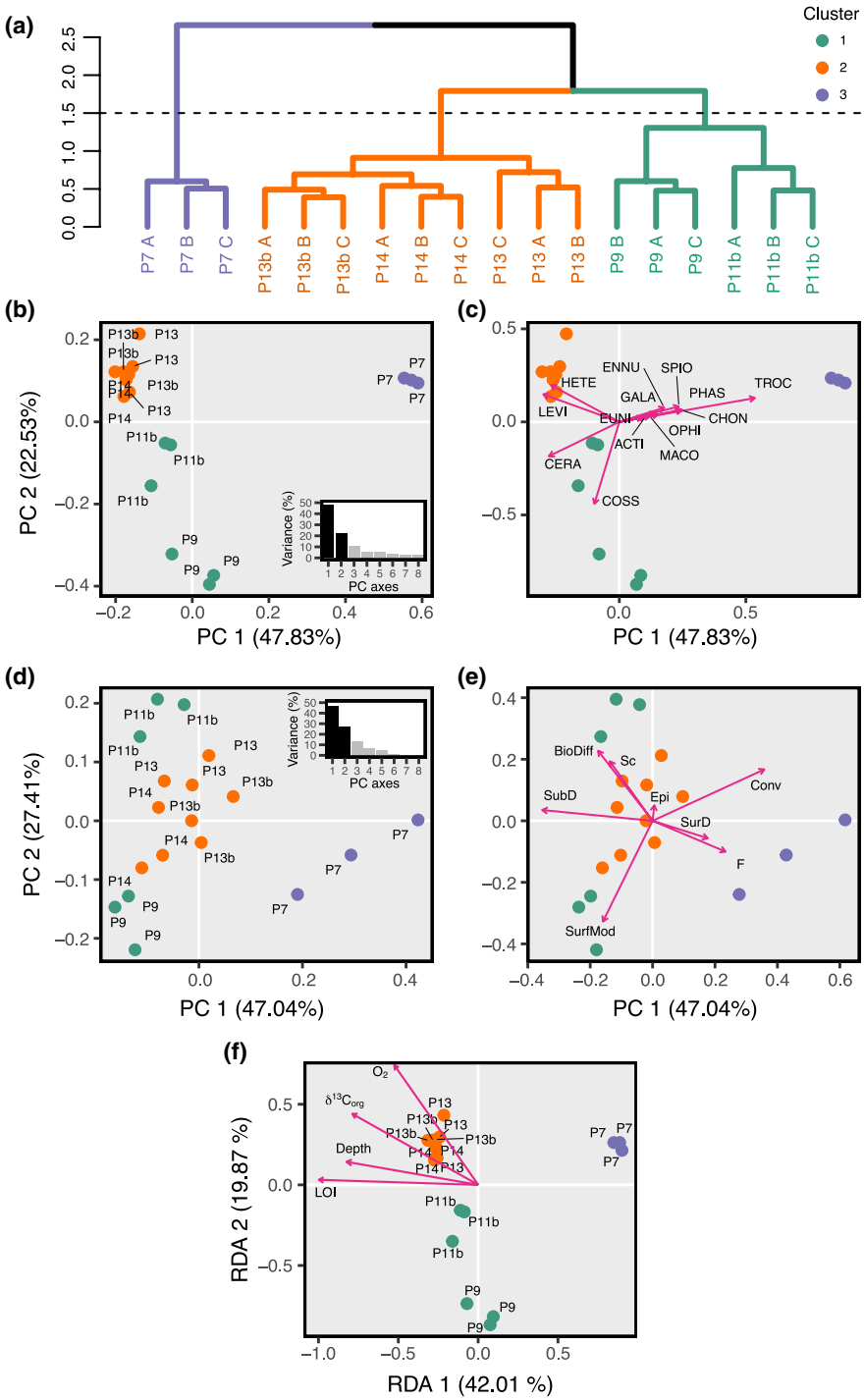

FIGURE 4 Macrobenthic community assemblage. (a) Hierarchical clustering and (b, c) principal component analyses of the Hellinger-transformed density of the macrofaunal species, and (d, e) traits and (f) redundancy analysis of the Hellinger-transformed density of the macrofauna of the six sampled stations. Panel (b, d) are depicted in scaling 1 to preserve the distance between stations and (c, e) in scaling 2 to preserve the correlation between species or functional traits. In (c), the only species for which the first two axes represented at least 30% (cumulative R^2) of their variance are depicted, ensuring that these species are well represented and did contribute to the observed pattern. Clusters determined in (a) are depicted in green for cluster 1, orange for cluster 2, and magenta for cluster 3. ACTI, *Actinaria*; CERA, *Ceratocephale loveni*; CHON, *Chone* spp.; COSS, *Cossura* spp.; ENNU, *Ennucula delphinodonta*; EUNI, *Eunice pennata*; GALA, *Galathowenia oculata*; HETE, *Heteromastus filiformis*; LEVI, *Levinsenia gracilis*; MACO, *Macoma calcarea*; OPHI, *Ophiura sarsii*; PHAS, *Phascolion* (*Phascilion*) *strombus strombus*; SPIO, *Spiophanes kroyeri*; TROC, *Ttrochochaeta watsoni*. See Table S1 for traits abbreviations.

to differences in LOI, depth and sediment $\delta^{13}C_{org}$ signature. The differences in macrobenthic community assemblage between clusters 1 and 2 were mainly related to $[O_2]_{bot}$. Within cluster 1, there was also segregation between stations P09 and P11b, related to $[O_2]_{bot}$.

3.4 | Bioturbation

Luminophore depth profiles showed very low within-station variability (Figure 5a). D_b coefficients were maximum at P07, minimum at P09 and P11b and intermediate at P13, P13b and P14 (Table S2; Figure 5b). The MPD was significantly lower at P07, P09 and P11B than at P13, P13b and P14. At all stations, except P09 and P11b, excess $[Br^-]$ depth profiles differed from the theoretical, purely diffusive profiles. Along the Laurentian Channel, the nonlocal bioirrigation coefficient (α) was highest at P07, drastically decreased at P09, then increased from P09 to P13, beyond which it remained relatively constant.

D_b and α are related to $[O_2]_{bot}$ in a significant non-linear relationship (Table S3; Figure 5e,g). D_b and α were relatively constant

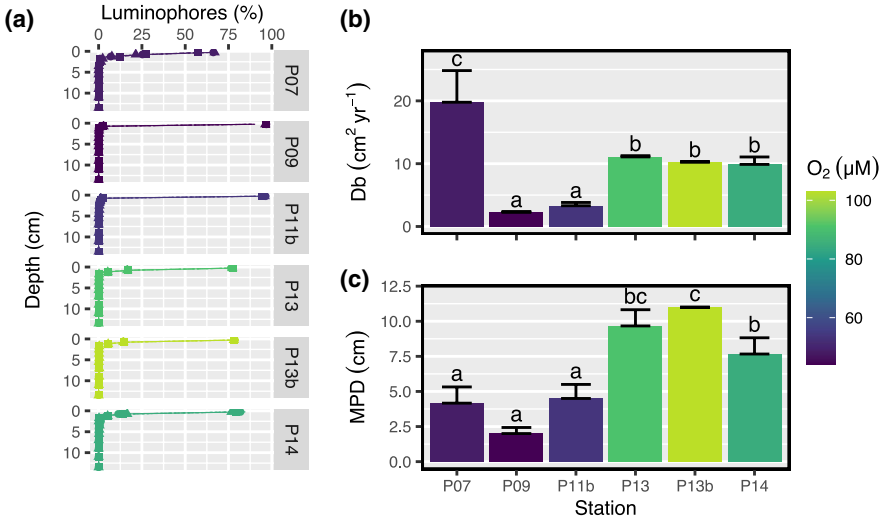

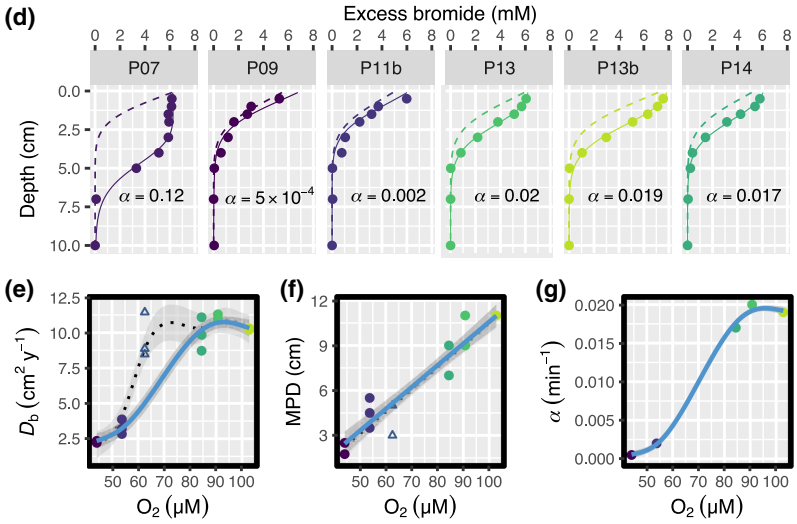

FIGURE 5 Bioturbation metrics. (a) Depth profiles of luminophore concentrations (points) and fitted models (lines) and (b) associated mean (±SD) biodiffusion coefficient (D_b; $n = 3$) and (c) maximum penetration depth (MPD; $n = 3$) of luminophores and (d) depth profile of dissolved bromide (points), fitted models (solid line) and theoretical diffusive profile (dashed lines). α (min^{-1}; $n = 1$) is given in the corresponding panel. (E–G) Generalized additive model (GAM) plots showing the effect of bottom-water O_2 concentration on bioturbation metrics excluding (blue curve) and including [dotted black curve in (e, f)] data from Cool (2022) (open triangle). Station P07 was excluded from GAM analyses, see text for details. Colour scale defines bottom-water O_2 concentration at the station. Letters indicate significant ($p < .05$) differences between stations.

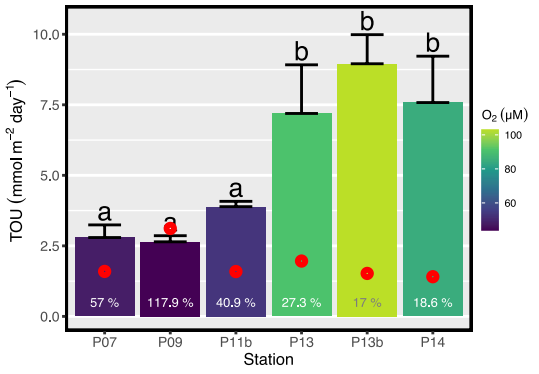

FIGURE 6 Sediment total oxygen uptake. Mean (±SD) sediment total oxygen uptake (TOU; $n = 3$). Colour scale defines bottom-water O_2 concentration at the station. Letters indicate significant differences between stations. Red circles depict the mean diffusive oxygen uptake (DOU, Figure 3b). Percentage values indicate the contribution of DOU to TOU.

at high $[O_2]_{bot}$ (≥80 µM) and abruptly dropped below an O_2 concentration of about 80 µM. MPD varied linearly with $[O_2]_{bot}$ (Figure 5f).

3.5 | Total oxygen uptake

Overall, TOU was significantly lower in the hypoxic area (i.e., P07, P09 and P11b) than in the non-hypoxic area (i.e., P13, P13b and P14) (Figure 6; Table S2). In addition, the DOU accounted for a larger proportion of the TOU in the hypoxic area (ranging from 40% to the totality of the TOU) while it accounted for only 17%–27% of the TOU in the non-hypoxic area.

4 | DISCUSSION

Like several coastal ecosystems, the EGSL bottom waters are subjected to persistent hypoxic conditions since the 1980s (Gilbert et al., 2005; Jutras et al., 2020, 2023). The areal extent and severity of hypoxia in this region have dramatically increased between 2018 and 2021, in response to changes in the circulation pattern in the western North Atlantic, likely due to climate change (Jutras et al., 2020, 2023). Although one cannot exclude the influence of eutrophication on bottom-water deoxygenation, this mechanism is

currently of secondary importance (Jutras et al., 2020). Accordingly, the sediment characteristics we documented are similar to those reported by Thibodeau et al. (2006) for the early 2000s, indicating stable OM inputs to the system over this period. In this study, we employed an integrative approach, involving marine biology, ecology, and biogeochemistry. For the first time, we shown evidence from a natural system that slow and persistently decreasing O_2 concentrations lead to a threshold-type response in bioturbation level, with far-reaching consequences on sediment biogeochemistry.

Early diagenetic processes in the sediment column are tightly linked to the environmental conditions in the overlying water column (Middelburg & Levin, 2009). We show that variations of the $[O_2]_{bot}$ alter the distribution of electron acceptors and associated early diagenetic reactions in the sediment column, but these changes do not occur gradually along the O_2 concentration gradient. The DOU remains relatively constant along the O_2 gradient except at the O_2-minimum location (P09), where DOU is about two times higher than at other stations. In a recent study, Cool (2022) showed that, along the $[O_2]_{bot}$ gradient, O_2 diffusing into the sediment was mainly consumed by the oxidation of reduced compounds produced below the oxic layer. This implies that OC mineralization results mainly from anaerobic diagenetic pathways. The OPD decreases linearly along the O_2 concentration gradient, restricting the already lower O_2 availability in the hypoxic area to the very first mm of the sediment column. Likewise, the concentration of NO_x in the overlying water and at the sediment surface (0.5 cm depth, corresponding to the peak NO_x concentration) decrease with $[O_2]_{bot}$, suggesting that the consumption of NO_x is not balanced by local benthic nitrification. The increase in pore-water SRP concentrations with depth tends to be larger and occurs at shallower depths in the hypoxic area (stations P09 and P11b) than in the non-hypoxic area (stations P13, P13b and P14). The vertical loss of SRP sediment adsorption capacity is typically attributed to the progressive reductive dissolution of iron-oxyhydroxides in the anoxic subsurface sediment layer and to the progressive remineralization of OM (Anschutz et al., 2007; Slomp, 2011; Sundby et al., 1992). In marine iron-rich sediments, such as those of the EGSL, the loss of sediment adsorption capacity probably results from squeezing the iron oxyhydroxide pool closer to the SWI (Lefort et al., 2012). Whereas Lefort et al. (2012) indicated that the reactive iron pool increases as the $[O_2]_{bot}$ decrease in the EGSL, the standing stock of iron-oxyhydroxides decreases at the expense of authigenic iron sulfides, more specifically acid volatile sulfides. However, our data cannot inform us about changes in the size of the standing stock of sedimentary iron-oxyhydroxides. Associated to these changes in the distribution of electron acceptors, our results show an accumulation of the reduced chemical compounds such as NH_4^+ in pore-waters, an acutely toxic compound to macrobenthic organisms (Gray et al., 2002).

Because macrobenthic biodiversity and species identity largely influence sedimentary OM mineralization (Snelgrove et al., 2018), identifying environmental factors that influence macrobenthic community assemblages is key to evaluate the effects of dissolved O_2 concentrations on ecosystem functioning. Total density as well as taxa and FRic decrease with decreasing $[O_2]_{bot}$ and substantially increase at the head of the EGSL. These results are consistent with those of previous studies in the EGSL (Belley et al., 2010; Zettler & Pollehne, 2023), as well as other low O_2 environments (Levin et al., 2009). Changes in macrobenthic community assemblages in the EGSL are driven by two environmental variables (Figure 4f). First, the quantity and origin of the sedimentary OM segregate the station at the head of the EGSL (station P07) from all other sampled stations. This station is the shallowest of the sampled sites and is characterized by coarser sediment, a lower sedimentary OM content, OC of mainly terrestrial origin (Table 1), and a higher sedimentation rate (Smith & Schafer, 1999). These features, and especially the latter, may explain the surprisingly greater proportion of large (>1 mm) organisms and the abundance of filter feeders (e.g., the Bivalvia *Ennucula deplphinodonta*, the Polychaeta *Chone* spp. and *Galathowenia oculata*) at this hypoxic location despite these traits being typically associated with taxa sensitive to low O_2 concentrations (Gammal et al., 2016; Levin, 2003; Levin et al., 2009). Second, $[O_2]_{bot}$ drives the differences in macrobenthic community assemblages between all the other stations along the EGSL. $[O_2]_{bot}$ has a direct effect on the survival of benthic organisms with threshold values depending on numerous factors (e.g., taxa, size, life history) (Diaz & Rosenberg, 1995; Vaquer-Sunyer & Duarte, 2008). Thus, bottom-water deoxygenation of the EGSL has prompted the migration and/or death of sensitive organisms. The low variability in macrobenthic community assemblages between stations within the non-hypoxic area (cluster 2), and the significant difference with those from the hypoxic area (cluster 3) suggest the existence of an O_2-dependent threshold below which macrobenthic community assemblages are significantly modified. According to our data, this $[O_2]_{bot}$ threshold occurs between 84 and 54 μM within the range of a previously reported threshold, between 100 and 50 μM, for benthic epifauna in the EGSL (Isabel et al., 2021).

Understanding how bioturbation rates will respond to decreasing $[O_2]_{bot}$ is of paramount importance to accurately and reliably predict the biogeochemical response of sediment to deoxygenation (Katsev et al., 2007; Middelburg & Levin, 2009). We show that $[O_2]_{bot}$ is an important driver of bioturbation processes. The MDP of luminophores decreases linearly with decreasing $[O_2]_{bot}$, suggesting that infauna responds to bottom-water deoxygenation by gradually reducing their burrowing depth, as reported in the paleorecord (Caswell & Herringshaw, 2022). In contrast, the relationships between $[O_2]_{bot}$ and particle mixing rate (D_b) and bioirrigation rate (α) are non-linear, as both show an abrupt change between 84 and 53 μM, implying the existence of an O_2-dependent threshold. Given that Cool (2022) reported a D_b of 9.6 $cm^2\,year^{-1}$ at a station near P09 that is characterized by a $[O_2]_{bot}$ of 63 μM, the threshold value appears to be located at the lower end of the O_2 window we identify. In the EGSL, the reduction of bioirrigation intensity below the O_2-dependent threshold led to the accumulation of pore-water NH_4^+. Interestingly, the depth at which the pore-water SRP concentration starts to increase is consistent with the MPD, suggesting that lowering of the MPD in the hypoxic area (stations P09 and

P11b) limits the production and the downward transport of metal oxides carrier phase. Overall, bioturbation seems to mitigate the effects of bottom-water hypoxia on sediment biogeochemistry as long as the $[O_2]_{bot}$ is above a threshold value that we estimate at around 63 μM.

The TOU decreases with $[O_2]_{bot}$ suggesting a lower influence of respiration and bioturbation by macrobenthic communities in the hypoxic area. This is consistent with our results on total macrofauna density and bioturbation rates. Interestingly, at station P09, the DOU accounted for all the TOU despite the non-negligible presence of macrofauna. The organisms inhabiting this particular station (the most abundant being annelid species) are clearly able to survive under low O_2 concentrations, as they likely possess adaptive traits enabling them to do so. Several coping strategies have been described tolerating hypoxia, such as the enhancement of an organism's O_2 uptake efficiency through increased respiratory surface area, higher concentration and/or affinity of respiratory pigments, lower metabolic rates (i.e., lower energy requirements) and the use of anaerobic metabolisms (Riedel et al., 2016; Spicer, 2016). Despite the latter being one of the most common responses to hypoxia (Childress & Seibel, 1998), it is mainly encountered in motile organisms that are able to reach more oxygenated water to balance their O_2 debts (Levin, 2003) or organisms that are subject to short-term, episodic hypoxic events (Hochachka & Somero, 2002). Given that our data suggest a very low macrofauna contribution to TOU, the physiological evolutionary strategy benthic invertebrates likely use in the hypoxic area investigated is to reduce their metabolic rates and activity levels. Indeed, annelids have been shown to adapt their metabolic rates and metabolism to global change drivers (Calosi et al., 2013; Thibault et al., 2020 and reference within), including hypoxia (Grimes et al., 2020). In the EGSL, as $[O_2]_{bot}$ have decreased at a relatively slow pace over the past century (Gilbert et al., 2005; Jutras et al., 2020, 2023), it may have allowed some species to establish themselves in the hypoxic area either through adaptation or because they already possessed hypoxia adaptive tolerance. However, the exact adaptive mechanism(s) that enable these species to flourish under chronic low O_2 conditions remain elusive.

Using a natural gradient of O_2 concentration, we shed some light on the hypoxia-induced effects on sediment biogeochemistry, benthic infauna community and benthic invertebrate activity levels in the EGSL. In contrast to our working hypothesis, macrobenthic community diversity and bioturbation rates decrease according to a threshold-type response with decreasing $[O_2]_{bot}$, a threshold that appears around 63 μM. Below this threshold particle mixing and bioirrigation decrease drastically to near null, likely in response to changes in infauna community assemblage and a lower activity of the species that inhabit these areas. Furthermore, our results suggest that the bioturbation activity of macrobenthic communities can buffer the effect of bottom-water deoxygenation on sediment biogeochemistry but when bioturbation decreases or ceases iron-oxyhydroxides are concentrated near the SWI and reduced compounds concentrations to build up in the sediment pore-waters. In marine iron-rich sediments such as in the EGSL, the large pool of iron-oxyhydroxides still serves as an oxidizing barrier and should do so as long as other electron acceptors of greater energy yields [e.g., O_2, NO_3^-, Mn(IV)-oxides] are not depleted (Katsev et al., 2007). Nevertheless, given the ongoing depletion of $[O_2]_{bot}$ in the EGSL (Jutras et al., 2023), as well as in the global ocean (Breitburg et al., 2018), we predict that these reduced compounds will continue to build up in pore-waters and progressively move closer to the SWI consuming electron acceptors, including metal oxyhydroxides and O_2. This will inevitably lead to a decrease in the stock of electron acceptors that act as an oxidizing barrier, until (once consumed) reduced compounds [such as Mn(II), Fe(II) and the toxic NH_4^+, As(III,IV) and HS^-] may diffuse out of the sediment column and further compromise the health of this ecosystem. Based on the space-for-time paradigm (Bozinovic et al., 2011; Gaston et al., 2009), our study of the EGSL deoxygenation gradient sheds light on what we may expect to observe in a deoxygenating ocean in the future, and its consequences for the ecological and biogeochemical functioning of benthic ecosystems.

AUTHOR CONTRIBUTIONS

Ludovic Pascal: Conceptualization; data curation; formal analysis; funding acquisition; investigation; methodology; project administration; software; supervision; validation; visualization; writing – original draft; writing – review and editing. **Joannie Cool:** Investigation. **Philippe Archambault:** Conceptualization; funding acquisition; methodology; resources; supervision; validation; writing – review and editing. **Piero Calosi:** Formal analysis; funding acquisition; project administration; validation; visualization; writing – review and editing. **André L. R. Cuenca:** Writing – review and editing. **Alfonso O. Mucci:** Validation; writing – review and editing. **Gwénaëlle Chaillou:** Conceptualization; formal analysis; funding acquisition; methodology; project administration; resources; supervision; validation; visualization; writing – review and editing.

ACKNOWLEDGMENTS

We thank the crew of the R/V *Coriolis II* for their help and dedication. We also thank Maxence St. Onge, Viridiana Jimenez and Claudie Meilleur for their assistance and support during the sampling; Lisa Treau De Coeli from Université Laval for her assistance in macrofauna identification; Karline Soetaert for her help with dissolved bromide modelling. LP is grateful to Sophie Moisset for her moral support. This work was financially supported by an FRQNT Team Grant (#285821) awarded to PA, PC and GC, with support from LP. Ship time was funded by the "programme Odyssée Saint Laurent" from the "Réseau Québec Maritime" awarded to GC, with support from LP. LP was supported by a B3X postdoctoral fellowship from FRQNT (#281864 and #322485) and a postdoctoral fellowship from MEOPAR (#PDF-25-2020). PA, PC, AOM and GC are supported by Natural Sciences and Engineering Research Council of Canada (NSERC) Discovery grants, respectively (RGPIN-2018-04982, RGPIN-2020-05627, RGPIN-2018-04421 and RGPIN-2018-556538).

CONFLICT OF INTEREST STATEMENT

The authors declare that the research was conducted in the absence of any commercial or financial relationships that could be construed as a potential conflict of interest.

DATA AVAILABILITY STATEMENT

The data that support the findings of this study are openly available in Dryad at https://doi.org/10.5061/dryad.6djh9w16w (Pascal et al., 2023).

ORCID

Ludovic Pascal https://orcid.org/0000-0002-9669-3336
Philippe Archambault https://orcid.org/0000-0001-5986-6149
Piero Calosi https://orcid.org/0000-0003-3378-2603
André L. R. Cuenca https://orcid.org/0000-0001-6091-2771
Alfonso O. Mucci https://orcid.org/0000-0001-9155-6319
Gwénaëlle Chaillou https://orcid.org/0000-0002-4170-8852

REFERENCES

Aminot, A., Kérouel, R., & Coverly, S. C. (2009). Nutrients in seawater using segmented flow analysis. In O. Wurl (Ed.), *Practical guidelines for the analysis of seawater* (p. 408). CRC Press. https://doi.org/10.1201/9781420073072

Anschutz, P., Chaillou, G., & Lecroart, P. (2007). Phosphorus diagenesis in sediment of the Thau lagoon. *Estuarine, Coastal and Shelf Science*, *72*(3), 447–456. https://doi.org/10.1016/j.ecss.2006.11.012

Belley, R., Archambault, P., & Sundby, B. (2010). Effects of hypoxia on benthic macrofauna and bioturbation in the Estuary and Gulf of St. Lawrence, Canada. *Continental Shelf Research*, *30*(12), 1302–1313. https://doi.org/10.1016/j.csr.2010.04.010

Benoit, P., Gratton, Y., & Mucci, A. (2006). Modeling of dissolved oxygen levels in the bottom waters of the Lower St. Lawrence Estuary: Coupling of benthic and pelagic processes. *Marine Chemistry*, *102*(1–2), 13–32. https://doi.org/10.1016/j.marchem.2005.09.015

Boudreau, B. P. (1984). On the equivalence of nonlocal and radial-diffusion models for porewater irrigation. *Journal of Marine Research*, *42*(1978), 731–735. https://doi.org/10.1357/002224084788505924

Boudreau, B. P. (1997). Chapter 4. Constitutive equations. In *Diagenetic models and their implementation: Modelling transport and reactions in aquatic sediments* (pp. 91–164). Springer. ISBN: 3540611258. https://doi.org/10.1007/978-3-642-60421-8

Bozinovic, F., Calosi, P., & Spicer, J. I. (2011). Physiological correlates of geographic range in animals. *Annual Review of Ecology, Evolution, and Systematics*, *42*, 155–179. https://doi.org/10.1146/annurev-ecolsys-102710-145055

Breitburg, D., Levin, L. A., Oschlies, A., Grégoire, M., Chavez, F. P., Conley, D. J., Garçon, V., Gilbert, D., Gutiérrez, D., Isensee, K., Jacinto, G. S., Limburg, K. E., Montes, I., Naqvi, S. W. A., Pitcher, G. C., Rabalais, N. N., Roman, M. R., Rose, K. A., Seibel, B. A., … Zhang, J. (2018). Declining oxygen in the global ocean and coastal waters. *Science (New York, N.Y.)*, *359*(6371), 7240. https://doi.org/10.1126/science.aam7240

Calosi, P., Rastrick, S. P. S., Lombardi, C., de Guzman, H. J., Davidson, L., Jahnke, M., Giangrande, A., Hardege, J. D., Schulze, A., Spicer, J. I., & Gambi, M.-C. (2013). Adaptation and acclimatization to ocean acidification in marine ectotherms: An in situ transplant experiment with polychaetes at a shallow CO_2 vent system. *Philosophical Transactions of the Royal Society B: Biological Sciences*, *368*(1627), 20120444. https://doi.org/10.1098/rstb.2012.0444

Caswell, B. A., & Herringshaw, L. (2022). Marine bioturbation collapse during early Jurassic deoxygenation: Implications for post-extinction marine ecosystem functioning. *Geological Society, London, Special Publications*, *529*, 311–344. https://doi.org/10.1144/SP529-2022-226

Chevenet, F., Doléadec, S., & Chessel, D. (1994). A fuzzy coding approach for the analysis of long-term ecological data. *Freshwater Biology*, *31*(3), 295–309. https://doi.org/10.1111/j.1365-2427.1994.tb01742.x

Childress, J. J., & Seibel, B. A. (1998). Life at stable low oxygen levels: Adaptations of animals to oceanic oxygen minimum layers. *Journal of Experimental Biology*, *201*(8), 1223–1232. https://doi.org/10.1242/jeb.201.8.1223

Cochran, J. K. (1985). Particle mixing rates in sediments of the eastern equatorial Pacific: Evidence from ^{210}Pb, ^{239,240}Pu and ^{137}Cs distributions at MANOP sites. *Geochimica et Cosmochimica Acta*, *49*(5), 1195–1210. https://doi.org/10.1016/0016-7037(85)90010-9

Cool, J. (2022). *Étude de la dynamique de l'oxygène dans les sédiments du chenal laurentien* (pp. 1–83). (M.Sc. thesis). Université du Québec à Rimouski.

Degen, R., & Faulwetter, S. (2019). The arctic traits database—A repository of arctic benthic invertebrate traits. *Earth System Science Data*, *11*(1), 301–322. https://doi.org/10.5194/essd-11-301-2019

Diaz, R. J., & Breitburg, D. L. (2009). Chapter 1: The hypoxic environment. In J. G. Richards, A. P. Farrell, & C. J. Brauner (Eds.), *Fish physiology* (Vol. *27*, pp. 1–23). Academic Press. https://doi.org/10.1016/S1546-5098(08)00001-0

Diaz, R. J., & Rosenberg, R. (1995). Marine benthic hypoxia: A review of its ecological effects and the behavioural response of benthic macrofauna. *Oceanography and Marine Biology: An Annual Review*, *33*, 245–303.

Diaz, R. J., & Rosenberg, R. (2008). Spreading dead zones and consequences for marine ecosystems. *Science (New York, N.Y.)*, *321*(5891), 926–929. https://doi.org/10.1126/science.1156401

Faulwetter, S., Markantonatou, V., Pavloudi, C., Papageorgiou, N., Keklikoglou, K., Chatzinikolaou, E., Pafilis, E., Chatzigeorgiou, G., Vasileiadou, K., Dailianis, T., Fanini, L., Koulouri, P., & Arvanitidis, C. (2014). Polytraits: A database on biological traits of marine polychaetes. *Biodiversity Data Journal*, *2*, e1024. https://doi.org/10.3897/bdj.2.e1024

Friedrich, J., Janssen, F., Aleynik, D., Bange, H. W., Boltacheva, N., Çagatay, M. N., Dale, A. W., Etiope, G., Erdem, Z., Geraga, M., Gilli, A., Gomoiu, M. T., Hall, P. O. J., Hansson, D., He, Y., Holtappels, M., Kirf, M. K., Kononets, M., Konovalov, S., … Wenzhöfer, F. (2014). Investigating hypoxia in aquatic environments: Diverse approaches to addressing a complex phenomenon. *Biogeosciences*, *11*(4), 1215–1259. https://doi.org/10.5194/bg-11-1215-2014

Froelich, P. N., Klinkhammer, G. P., Bender, M. L., Luedtke, N. A., Hearth, G. R., Cullen, D., Dauphin, P., Hammond, D., Hartman, B., & Maynard, V. (1979). Early oxidation of organic matter in pelagic sediments of the eastern equatorial Atlantic: Suboxic diagenesis. *Geochimica et Cosmochimica Acta*, *43*, 1075–1090. https://doi.org/10.1016/0016-7037(79)90095-4

Gammal, J., Norkko, J., Pilditch, C. A., & Norkko, A. (2016). Coastal hypoxia and the importance of benthic macrofauna communities for ecosystem functioning. *Estuaries and Coasts*, *40*(2), 457–468. https://doi.org/10.1007/s12237-016-0152-7

Gaston, K. J., Chown, S. L., Calosi, P., Bernardo, J., Bilton, D. T., Clarke, A., Clusella-Trullas, S., Ghalambor, C. K., Konarzewski, M., Peck, L. S., Porter, W. P., Pörtner, H. O., Rezende, E. L., Schulte, P. M., Spicer, J. I., Stillman, J. H., Terblanche, J. S., & van Kleunen, M. (2009). Macrophysiology: A conceptual reunification. *The American Naturalist*, *174*(5), 595–612. https://doi.org/10.1086/605982

Gilbert, D. (2004). *Propagation of temperature signals from the northwest Atlantic continental shelf edge into the Laurentian Channel*. ICES CM, N(07).

Gilbert, D., Sundby, B., Gobeil, C., Mucci, A., & Tremblay, G.-H. (2005). A seventy-two-year record of diminishing deep-water oxygen in the St. Lawrence estuary: The northwest Atlantic connection. *Limnology and Oceanography*, *50*(5), 1654–1666. https://doi.org/10.4319/lo.2005.50.5.1654

Glud, R. N. (2008). Oxygen dynamics of marine sediments. *Marine Biology Research*, *4*(4), 243–289. https://doi.org/10.1080/17451000801888726

Grasshoff, K., & Ehrhardt, M. (1999). *Methods of seawater analysis*. Wiley-VCH.

Gray, J., Wu, R., & Or, Y. (2002). Effects of hypoxia and organic enrichment on the coastal marine environment. *Marine Ecology Progress Series*, *238*, 249–279. https://doi.org/10.3354/meps238249

Grimes, C. J., Capps, C., Petersen, L. H., & Schulze, A. (2020). Oxygen consumption during and post-hypoxia exposure in bearded fireworms (Annelida: Amphinomidae). *Journal of Comparative Physiology. B, Biochemical, Systemic, and Environmental Physiology*, *190*(6), 681–689. https://doi.org/10.1007/s00360-020-01308-y

Hochachka, P. W., & Somero, G. N. (2002). Influence of oxygen availability. In *Biochemical adaptation: Mechanism and process in physiological evolution* (1st ed., p. 480). Oxford University Press. ISBN: 0195117034.

Isabel, L., Beauchesne, D., McKindsey, C., & Archambault, P. (2021). Detection of ecological thresholds and selection of indicator taxa for epibenthic communities exposed to multiple pressures. *Frontiers in Marine Science*, *8*, 720710. https://doi.org/10.3389/fmars.2021.720710

Johnson, M. D., Scott, J. J., Leray, M., Lucey, N., Bravo, L. M. R., Wied, W. L., & Altieri, A. H. (2021). Rapid ecosystem-scale consequences of acute deoxygenation on a Caribbean coral reef. *Nature Communications*, *12*(1), 4522. https://doi.org/10.1038/s41467-021-24777-3

Jutras, M., Dufour, C. O., Mucci, A., Cyr, F., & Gilbert, D. (2020). Temporal changes in the causes of the observed oxygen decline in the St. Lawrence estuary. *Journal of Geophysical Research: Oceans*, *125*(12), 16577. https://doi.org/10.1029/2020JC016577

Jutras, M., Mucci, A., Chaillou, G., Nesbitt, W. A., & Wallace, D. W. R. (2023). Temporal and spatial evolution of bottom-water hypoxia in the St. Lawrence estuarine system. *Biogeosciences*, *20*(4), 839–849. https://doi.org/10.5194/bg-20-839-2023

Katsev, S., Chaillou, G., Sundby, B., & Mucci, A. (2007). Effects of progressive oxygen depletion on sediment diagenesis and fluxes: A model for the lower St. Lawrence River Estuary. *Limnology and Oceanography*, *52*(6), 2555–2568. https://doi.org/10.4319/lo.2007.52.6.2555

Kelley, D., & Richards, C. (2022). *oce: Analysis of oceanographic data* [computer software]. https://CRAN.R-project.org/package=oce

Kristensen, E., Penha-Lopes, G., Delefosse, M., Valdemarsen, T., Quintana, C., & Banta, G. (2012). What is bioturbation? The need for a precise definition for fauna in aquatic sciences. *Marine Ecology Progress Series*, *446*, 285–302. https://doi.org/10.3354/meps09506

Laliberté, E., & Legendre, P. (2010). A distance-based framework for measuring functional diversity from multiple traits. *Ecology*, *91*(1), 299–305. https://doi.org/10.1890/08-2244.1

Lefort, S., Mucci, A., & Sundby, B. (2012). Sediment response to 25 years of persistent hypoxia. *Aquatic Geochemistry*, *18*(6), 461–474. https://doi.org/10.1007/s10498-012-9173-4

Lepore, B. J., & Barak, P. (2009). A colorimetric microwell method for determining bromide concentrations. *Soil Science Society of America Journal*, *73*(4), 1130–1136. https://doi.org/10.2136/sssaj2007.0226

Levin, L. A. (2003). Oxygen minimum zone benthos: Adaptation and community response to hypoxia. In R. N. Gibson & R. J. A. Atkinson (Eds.), *Oceanography and marine biology, an annual review* (Vol. *41*, pp. 1–45). Springer.

Levin, L. A., Ekau, W., Gooday, A. J., Jorissen, F., Middelburg, J. J., Naqvi, S. W. A., Neira, C., Rabalais, N. N., & Zhang, J. (2009). Effects of natural and human-induced hypoxia on coastal benthos. *Biogeosciences*, *6*(10), 2063–2098. https://doi.org/10.5194/bg-6-2063-2009

Lohrer, A. M., Thrush, S. F., & Gibbs, M. M. (2004). Bioturbators enhance ecosystem function through complex biogeochemical interactions. *Nature*, *431*(7012), 1092–1095. https://doi.org/10.1038/nature03042

Martin, W. R., & Banta, G. T. (1992). The measurement of sediment irrigation rates: A comparison of the Br^- tracer and $^{222}Rn/^{226}Ra$ disequilibrium techniques. *Journal of Marine Research*, *50*(1), 125–154. https://doi.org/10.1357/002224092784797737

Meysman, F. J. R., Middelburg, J. J., & Heip, C. H. R. (2006). Bioturbation: A fresh look at Darwin's last idea. *Trends in Ecology & Evolution*, *21*(12), 688–695. https://doi.org/10.1016/j.tree.2006.08.002

Middelburg, J. J., & Levin, L. (2009). Coastal hypoxia and sediment biogeochemistry. *Biogeosciences*, *6*, 1273–1293. https://doi.org/10.5194/bg-6-1273-2009

Norkko, J., Pilditch, C. A., Gammal, J., Rosenberg, R., Enemar, A., Magnusson, M., Granberg, M. E., Lindgren, J. F., Agrenius, S., & Norkko, A. (2019). Ecosystem functioning along gradients of increasing hypoxia and changing soft-sediment community types. *Journal of Sea Research*, *153*, 101781. https://doi.org/10.1016/j.seares.2019.101781

Oksanen, J., Simpson, G. L., Blanchet, F. G., Kindt, R., Legendre, P., Minchin, P. R., O'Hara, R. B., Solymos, P., Stevens, M. H. H., Szoecs, E., Wagner, H., Barbour, M., Bedward, M., Bolker, B., Borcard, D., Carvalho, G., Chirico, M., De Caceres, M., Durand, S., … Weedon, J. (2022). *vegan: Community ecology package* [computer software]. https://CRAN.R-project.org/package=vegan

Pascal, L., Cool, J., Archambault, P., Calosi, P., Cuenca, A. L. R., Mucci, A. O., & Chaillou, G. (2023). Data from: Ocean deoxygenation caused non-linear responses in the structure and functioning of benthic ecosystems (Version 2, p. 51666920 bytes) [dataset]. *Dryad*. https://doi.org/10.5061/dryad.6djh9w16w

Petrie, B., Drinkwater, K., Sandstrom, A., Pettipas, R., Gregory, D., Gilbert, D., & Sekhon, P. (1996). Temperature, salinity and sigma-t atlas for the Gulf of St. Lawrence. *Canadian Technical Report of Hydrography and Ocean Sciences*, *178*, 256. https://waves-vagues.dfo-mpo.gc.ca/library-bibliotheque/198079.pdf

Queirós, A. M., Birchenough, S. N. R., Bremner, J., Godbold, J. A., Parker, R. E., Romero-Ramirez, A., Reiss, H., Solan, M., Somerfield, P. J., Colen, C. V., Hoey, G. V., & Widdicombe, S. (2013). A bioturbation classification of European marine infaunal invertebrates. *Ecology and Evolution*, *3*(11), 3958–3985. https://doi.org/10.1002/ece3.769

R Core Team. (2022). *R: A language and environment for statistical computing* [Computer software]. https://www.R-project.org/

Rabalais, N. N., Díaz, R. J., Levin, L. A., Turner, R. E., Gilbert, D., & Zhang, J. (2010). Dynamics and distribution of natural and human-caused hypoxia. *Biogeosciences*, *7*(2), 585–619. https://doi.org/10.5194/bg-7-585-2010

Riedel, B., Diaz, R., Rosenberg, R., & Stachowitsch, M. (2016). The ecological consequences of marine hypoxia: From behavioural to ecosystem responses. In M. Solan & N. M. Whiteley (Eds.), *Stressors in the marine environment* (pp. 175–194). Oxford University Press. https://doi.org/10.1093/acprof:oso/9780198718826.003.0010

Riedel, B., Pados, T., Pretterebner, K., Schiemer, L., Steckbauer, A., Haselmair, A., Zuschin, M., & Stachowitsch, M. (2014). Effect of hypoxia and anoxia on invertebrate behaviour: Ecological perspectives from species to community level. *Biogeosciences*, *11*(6), 1491–1518. https://doi.org/10.5194/bg-11-1491-2014

Slomp, C. P. (2011). Phosphorus cycling in the estuarine and coastal zones. In R. W. P. M. Laane & J. J. Middelburg (Eds.), *Treatise on estuarine and coastal science* (pp. 201–229). Elsevier. https://doi.org/10.1016/b978-0-12-374711-2.00506-4

Smith, J. N., & Schafer, C. T. (1999). Sedimentation, bioturbation, and Hg uptake in the sediments of the estuary and Gulf of St. Lawrence. *Limnology and Oceanography*, *44*(1), 207–219. https://doi.org/10.4319/lo.1999.44.1.0207

Snelgrove, P. V. R., Soetaert, K., Solan, M., Thrush, S., Wei, C.-L., Danovaro, R., Fulweiler, R. W., Kitazato, H., Ingole, B., Norkko, A., Parkes, R. J., & Volkenborn, N. (2018). Global carbon cycling on a heterogeneous seafloor. *Trends in Ecology & Evolution*, *33*(2), 96–105. https://doi.org/10.1016/j.tree.2017.11.004

Soetaert, K., & Meysman, F. J. R. (2012). Reactive transport in aquatic ecosystems: Rapid model prototyping in the open source software R. *Environmental Modelling & Software*, *32*, 49–60. https://doi.org/10.1016/j.envsoft.2011.08.011

Soetaert, K., Petzoldt, T., & Setzer, R. W. (2010). Solving differential equations in R: Package deSolve. *Journal of Statistical Software*, *33*(9), 1–25. https://doi.org/10.18637/jss.v033.i09

Spicer, J. I. (2016). Respiratory responses of marine animals to environmental hypoxia. In M. Solan & N. Whiteley (Eds.), *Stressors in the marine environment: Physiological and ecological responses; societal implications* (pp. 22–35). Oxford University Press. https://doi.org/10.1093/acprof:oso/9780198718826.003.0002

Stockdale, A., Davison, W., & Zhang, H. (2009). Micro-scale biogeochemical heterogeneity in sediments: A review of available technology and observed evidence. *Earth-Science Reviews*, *92*(1–2), 81–97. https://doi.org/10.1016/j.earscirev.2008.11.003

Sundby, B., Gobeil, C., Silverberg, N., & Mucci, A. (1992). The phosphorus cycle in coastal marine sediments. *Limnology and Oceanography*, *37*(6), 1129–1145. https://doi.org/10.4319/lo.1992.37.6.1129

Thibault, C., Massamba-N'Siala, G., Noisette, F., Vermandele, F., Babin, M., & Calosi, P. (2020). Within- and trans-generational responses to combined global changes are highly divergent in two congeneric species of marine annelids. *Marine Biology*, *167*(4), 41. https://doi.org/10.1007/s00227-019-3644-8

Thibodeau, B., de Vernal, A., & Mucci, A. (2006). Recent eutrophication and consequent hypoxia in the bottom waters of the Lower St. Lawrence Estuary: Micropaleontological and geochemical evidence. *Marine Geology*, *231*(1–4), 37–50. https://doi.org/10.1016/j.margeo.2006.05.010

Thibodeau, B., Not, C., Zhu, J., Schmittner, A., Noone, D., Tabor, C., Zhang, J., & Liu, Z. (2018). Last century warming over the Canadian Atlantic shelves linked to weak Atlantic meridional overturning circulation. *Geophysical Research Letters*, *45*(22), 12376–12385. https://doi.org/10.1029/2018GL080083

Van Cappellen, P., & Wang, Y. (1996). Cycling of iron and manganese in surface sediments; a general theory for the coupled transport and reaction of carbon, oxygen, nitrogen, sulfur, iron, and manganese. *American Journal of Science*, *296*(3), 197–243. https://doi.org/10.2475/ajs.296.3.197

Vaquer-Sunyer, R., & Duarte, C. M. (2008). Thresholds of hypoxia for marine biodiversity. *Proceedings of the National Academy of Sciences of the United States of America*, *105*(40), 15452–15457. https://doi.org/10.1073/pnas.0803833105

Villéger, S., Mason, N. W. H., & Mouillot, D. (2008). New multidimensional functional diversity indices for a multifaceted framework in functional ecology. *Ecology*, *89*(8), 2290–2301. https://doi.org/10.1890/07-1206.1

Volkenborn, N., Woodin, S. A., Wethey, D. S., & Polerecky, L. (2019). Bioirrigation. In J. K. Cochran, H. J. Bokuniewicz, & P. L. Yager (Eds.), *Encyclopedia of ocean sciences* (3rd ed., pp. 663–670). Academic Press. https://doi.org/10.1016/B978-0-12-409548-9.09525-7

Wood, S. N. (2017). *Generalized additive models: An introduction with R* (2nd ed.). Chapman and Hall/CRC. https://doi.org/10.1201/9781315370279

Zettler, M. L., & Pollehne, F. (2023). Macrozoobenthic diversity along an oxygen gradient in the deep trough of the Gulf of St. Lawrence (Canada). *Diversity*, *15*(7), Article 7. https://doi.org/10.3390/d15070854

SUPPORTING INFORMATION

Additional supporting information can be found online in the Supporting Information section at the end of this article.

How to cite this article: Pascal, L., Cool, J., Archambault, P., Calosi, P., Cuenca, A. L. R., Mucci, A. O., & Chaillou, G. (2023). Ocean deoxygenation caused non-linear responses in the structure and functioning of benthic ecosystems. *Global Change Biology*, *00*, e16994. https://doi.org/10.1111/gcb.16994